Electrochimica Acta 55 (2010) 895–902

Contents lists available at ScienceDirect

Electrochimica Acta

journal homepage: www.elsevier.com/locate/electacta

A series of LiI/acetamide phase transition electrolytes and their applications in dye-sensitized solar cells

Zhexun Yu, Hong Li, Kexin Li, Da Qin, Minghui Deng, Dongmei Li, Yanhong Luo, Qingbo Meng*, Liquan Chen

Beijing National Laboratory for Condensed Matter Physics, Institute of Physics, Chinese Academy of Sciences, 100190 Beijing, China

ARTICLE INFO

Article history:
Received 15 July 2009
Received in revised form
11 September 2009
Accepted 16 September 2009
Available online 23 September 2009

Keywords:
Phase transition
LiI/acetamide
Nano-SiO_2
Crystallization
Dye-sensitized solar cell

ABSTRACT

A new series of electrolytes composed of LiI and acetamide have been investigated in dye-sensitized solar cells (DSSCs). These electrolytes melt at about 50 °C and their ionic conductivities vary drastically below and above the melting points (T_m). They tend to form large crystals at low temperature, leading to poor penetration and contact within porous TiO_2 anode film. This shortage is improved by introducing nano-SiO_2 particles into the electrolyte. A total conversion efficiencies (η) of 0.3% at 35 °C and 4.2% at 75 °C are achieved respectively under AM 1.5 simulated solar light illumination when a LiI/acetamide (1:16) electrolyte with 8 wt% nano-SiO_2 is used. It is expected that the DSSC using phase transition electrolyte could show high efficiency for operation at high temperature and high stability for storage at low temperature.

1. Introduction

Dye-sensitized solar cell (DSSC) using nonaqueous electrolyte shows moderate light to electricity conversion efficiency (11%) but low cost [1–3]. It is a very attractive photovoltaic device for large scale application. However, leakage and volatility of organic solvents during long term operation under high temperature may decrease the performances. In order to solve this problem, tight sealing technology has to be developed. On the other hand, more approaches are paid to develop solid DSSC, such as using p-type semiconductors [4–6], organic hole transport medium [7,8], polymer electrolytes [9–15], additional compounds [16–20], and ionic liquids [21–23].

The LiX/acetamide electrolytes have been developed for Li-ion batteries previously [24–26]. Most of these electrolytes are liquid at room temperature except the LiBOB (lithium bis(oxalato)borate)/acetamide system (molar ratio 1:8) [27], which shows a melting point around 42 °C. Here we report that the LiI/acetamide electrolytes reveal similar phase transition behaviors as the LiBOB/acetamide electrolytes. For the first time, the phase transition electrolytes are tested in DSSC. This is different with pure solid or liquid electrolytes mentioned above. It is expected that the electrode/electrolyte contact and ionic conductivity of the electrolyte can be greatly improved during operation at high temperature in liquid state and keep high stability during storage at low temperature in solid state.

2. Experimental

2.1. Preparation of the electrolytes

Certain amount of anhydrous LiI (Wako) and acetamide (≥98.5%, Beijing Chemical Reagents Company) was mixed together with the required molar ratio (for example, 1:16 LiI/acetamide electrolyte means 0.0306 g LiI and 0.2161 g acetamide) in an argon-filled glove box (M. Braun). Then the mixture was heated to about 90 °C, which is higher than the melting point (T_m) of the acetamide of 81 °C. Then it was stirred until a homogeneous solution was obtained. After cooling down to room temperature naturally, the solid-state electrolyte was formed. The electrolytes containing ceramic oxides were also prepared by adding the additives into the above solutions and stirring vigorously until a homogeneous composite was formed. The morphology of the electrolytes on the TiO_2 electrode film was investigated by a scanning electron microscope (FEI, S-FEG, XL30).

2.2. Differential scanning calorimeter (DSC) measurement

The thermal properties of the electrolytes were characterized on a differential scanning calorimeter (NETSCH STA 449C) between

* Corresponding author. Tel.: +86 10 8264 9242; fax: +86 10 8264 9242.
E-mail address: qbmeng@aphy.iphy.ac.cn (Q. Meng).

0013-4686/$ – see front matter © 2009 Elsevier Ltd. All rights reserved.
doi:10.1016/j.electacta.2009.09.050

room temperature and 100 °C by sealing 5 mg of the LiI/acetamide electrolyte in an aluminum pan in the glove box. The pan with the electrolyte was heated at a rate of 5 °C/min in argon atmosphere.

2.3. Infrared absorption spectra

Infrared absorption spectra were recorded on a Fourier transform infrared (FTIR) spectrometer (Bruker Tensor 27). The LiI/acetamide electrolyte was mixed with KBr and pressed into a pellet in the glove box. The pellet was taken out immediately and was transferred into the FTIR instrument. Each of the IR spectra was the average of 20 scans (each scan cost 2 s).

2.4. Ionic conductivity measurement

The ionic conductivities of the electrolytes were determined by ac impedance technique on an IM6ex electrochemical work station (ZAHNER) from 5 Hz to 3 MHz between room temperature and 85 °C in a sealed cell with a sandwich structure of "stainless steel/electrolyte/stainless steel". The cell was assembled in the glove box by heating the electrolyte to melt. The sample had been kept at each temperature for an hour before each measurement.

2.5. TiO_2/dye film preparation

The nanocrystalline TiO_2 film was fabricated by a doctor-blading technique according to the literature [28]. The TiO_2 (P25) paste was deposited on a conducting glass substrate (F-doped SnO_2, 15 Ω/□), followed by sintering at 450 °C for 30 min. Large TiO_2 particles (about 150 nm, 16.7 wt%) were introduced into the paste to scatter the incident light as well as to obtain large vacancies. The thickness of the film was about 10 μm. The mesoporous TiO_2 film was preheated at 120 °C for 30 min before it was immersed into a solution of the dye cis-dithiocyanate-N,N′-bis (4,4′-dicarboxylate-2,2′-bipyridine) ruthenium(II) (RuN3, Solaronix) with a concentration of 3×10^{-4} M in dry ethanol overnight.

2.6. Fabrication of the DSSCs

The electrolytes were firstly dissolved in a mixture of propylene carbonate (PC) and dimethyl carbonate (DMC) (Battery Grade, 1:3, v/v) and stirred vigorously for 30 min. Then a droplet of the electrolyte solution was dropped onto the surface of the dye covered TiO_2 film. The solvents were removed under vacuum condition at room temperature. The same procedure was repeated several times until the TiO_2 film was covered with the electrolyte. There was no residual PC in the electrolyte as demonstrated by the FTIR experiment. Finally, an open sandwich-type cell was fabricated in air by clamping the TiO_2 electrode with a platinized FTO counter electrode (sputtered Pt mirror) with two clips. The active electrode area was 0.15 cm^2.

2.7. Photoelectrochemical measurement

A solar light simulator (Oriel, 91192) was used to give an illumination of 100 mW cm^{-2} (AM 1.5) on the surface of the solar cells. The incident light intensity was measured with a radiant power/energy meter (Oriel, 70260) before each experiment. The characteristics of the photocurrent density–photovoltage of the cell under these conditions were recorded by a potentiostat (Princeton Applied Research, Model 263A). The cells were tested under different temperatures using a hot plate (PMC 732 SERIES). The dark currents were measured under the same conditions in dark. The electrochemical impedance spectroscopy (EIS) measurements were performed with an IM6ex electrochemical work station (ZAHNER) with the frequency range from 100 mHz to 100 kHz. The magnitude of the alternative signal was 10 mV. The impedance measurements were carried out under forward bias of 0.75 V in the dark.

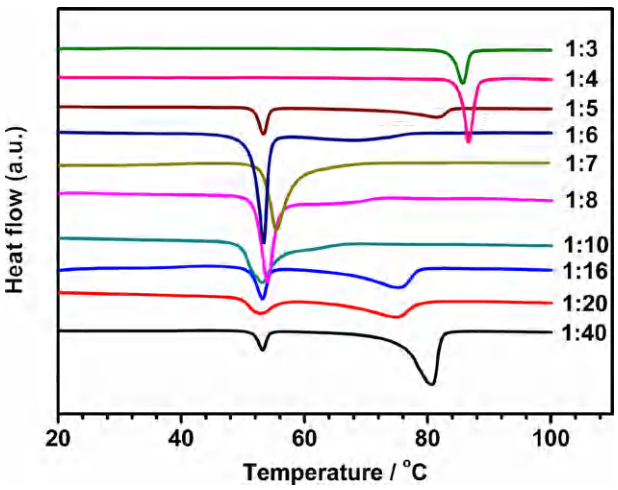

Fig. 1. DSC curves of the LiI/acetamide system with different molar ratios (LiI/acetamide).

3. Results and discussion

3.1. Thermal properties of the LiI/acetamide electrolytes

Pure LiI and acetamide melt at 447 and 81 °C, respectively. The melting points decrease after mixing. Fig. 1 shows the differential scanning calorimeter (DSC) curves of LiI/acetamide system with different molar ratios (LiI/acetamide) between 20 and 100 °C. As seen in Fig. 1, there is only one endothermic peak in each DSC curve when the molar ratio ranges from 1:10 to 1:6 and from 1:4 to 1:3. Two peaks can be observed in the samples beyond the molar ratio range, indicating the existence of liquid–solid coexistence regime between 50 and 80 °C. The appearance of eutectic temperature around 50 °C for the electrolytes at certain molar ratio indicates the existence of the interaction between the lithium salt and acetamide, as further shown in following FTIR results.

3.2. IR studies

FTIR spectra of pure acetamide and the electrolytes with different LiI/acetamide molar ratios are shown in Fig. 2. Solid acetamide usually exists in the form of dimer or polymer due to the intermolecular hydrogen bonding [29]. There is a very strong broad peak at about 3375 cm^{-1} in its IR spectrum, corresponding to the asymmetric stretching vibration band of the amido group. As shown in Fig. 3(a), when LiI is gradually added into acetamide, the peak at 3375 cm^{-1} shifts slightly towards higher wavenumber and a new peak which corresponds to the free N–H stretch at 3450 cm^{-1} appears [30]. This is caused by the impairing of the hydrogen bonds in acetamide due to the interactions between the Li ions and acetamide.

The peak at 1670 cm^{-1} is ascribed to the absorption of the amide vibration band from carbonyl group (Fig. 3(b)). It red-shifts slightly from 1670 to 1653 cm^{-1} when the concentration of LiI increases. This is also caused by the coordination interactions between Li^+ and the C=O group. Similar phenomenon has been reported in the LiTFSI ($LiN(SO_2CF_3)_2$)/acetimide [24,25] and LiBETI ($LiN(SO_2C_2F_5)_2$)/acetamide system [26]. However, the peak shifts in those systems are much more significant [25,26]. In those cases,

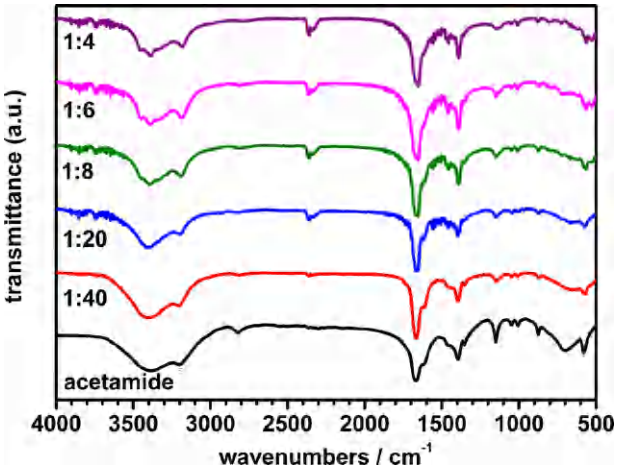

Fig. 2. FTIR spectra of the LiI/acetamide electrolytes with different molar ratios.

lithium salts can react with acetamide spontaneously forming liquid electrolytes at room temperature. On the contrary, the mixture of LiI and acetamide at ambient conditions do not transform into liquid spontaneously, indicating relatively weak coordination interactions between LiI and acetamide.

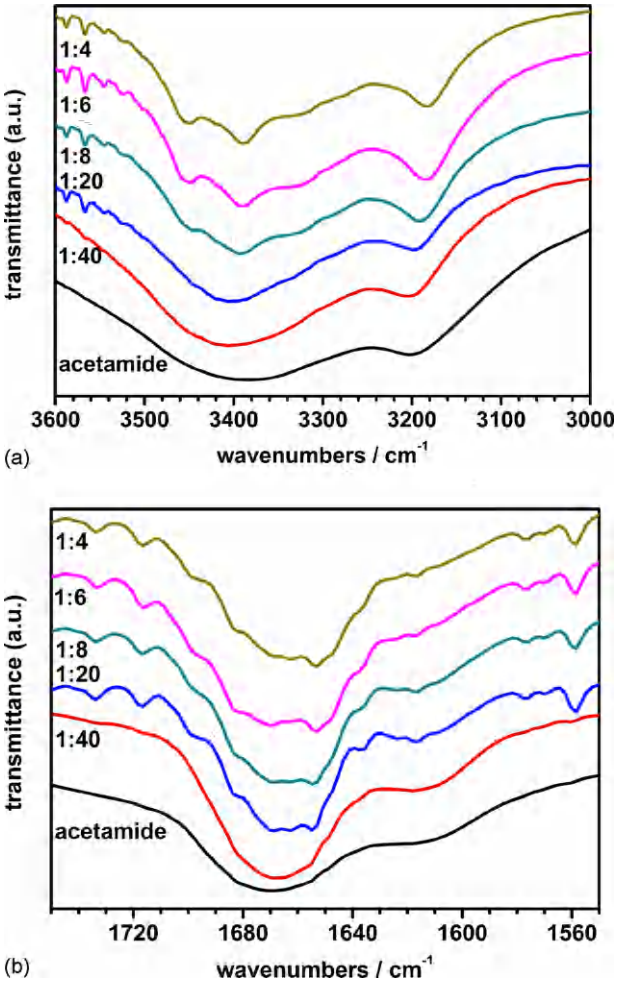

Fig. 3. FTIR spectra of the LiI/acetamide system with different molar ratios: (a) 3600–3000 cm^{-1} and (b) 1750–1550 cm^{-1}.

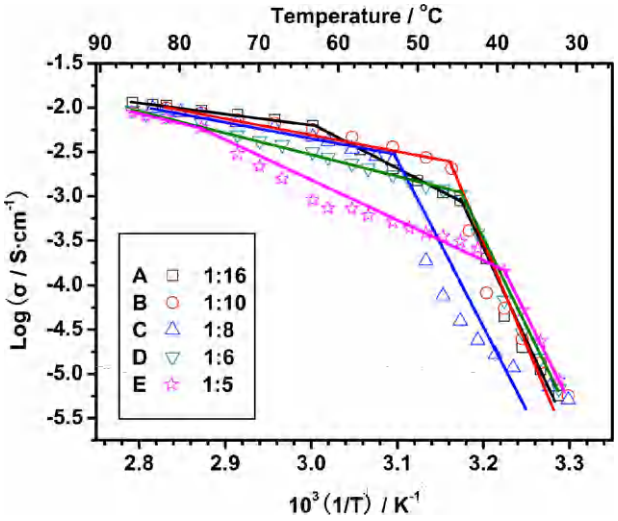

Fig. 4. Temperature-dependent conductivities of different electrolytes (heating process). Symbol: the data points; line: the fitted curves.

3.3. Ionic conductivities of the electrolytes

Fig. 4 shows the conductivities of different electrolytes in a temperature range from 30 to 85 °C. For the electrolytes B, C and D, two slopes in the Arrhenius plots can be found while the electrolytes A and E show three slopes, suggesting that two phase transition processes occur within the whole temperature range. This is consistent with the DSC results.

The activation energies (*Ea*) for different electrolytes are summarized in Table 1. We can see that the electrolyte A exhibits the highest activation energy in the low temperature range but the lowest, which is close to that of the liquid electrolyte (ca. 14.5 kJ mol^{-1}) reported in Ref. [31], in the high temperature region. The conductivity of electrolyte A at 80 °C, as shown in Fig. 4, has exceeded 1.0×10^{-2} S cm^{-1}.

Supercooling phenomenon is observed in LiI/acetamide electrolytes. As shown in Fig. 5(a), the electrolyte A melts at 51 °C and freezes at 40 °C. In Fig. 5(b), the melting point of the electrolyte D is 51 °C and it does not solidify at a rate of 5 °C/min during cooling down. This phenomenon is also observed in the conductivity results. As indicated in Fig. 5(c) and (d), the conductivities of the electrolytes in the cooling process (cooling down naturally) are higher than that in the heating process at the same temperature, especially in the low temperature region. The supercooling phenomenon is also found in other salt–acetamide systems [27,32]. The kinetics of supercooling needs further investigations.

3.4. Effect of nano-SiO_2 on the performance of DSSC

Application of electrolyte A (LiI/acetamide = 1:16) on DSSCs has been investigated due to its high conductivity in the high temperature range. The cells were heated at a rate of about 1 °C/min, and they will be kept at the testing temperature for at least 5 min before each measurement. The detailed cell performances are listed in Table 2.

It can be seen in Table 2 that the J_{sc} increases remarkably as the temperature arises (especially higher than 45 °C), which is in accordance with the conductivity–temperature behavior (the black line in Fig. 4). After reaching a peak value of 5.40 mA cm^{-2}, the J_{sc} decreases slightly. This is probably due to the incremental electron loss at the TiO_2/electrolyte interface. The V_{oc} also increases firstly but drops down quickly when the temperature is higher, which is caused by the decline of the Fermi-level (TiO_2) as well as the ascent

Table 1
The activation energies (*Ea*) comparison of different electrolytes in different temperature ranges.

Symbol	Electrolyte molar ratio (LiI/acetamide)	*Ea* (kJ mol^{-1})		
		High temperature	Middle temperature	Low temperature
A	1:16	23.8	95.0	371
B	1:10	37.4		343
C	1:8	40.0		216
D	1:6	48.4		368
E	1:5	39.8	76.7	362

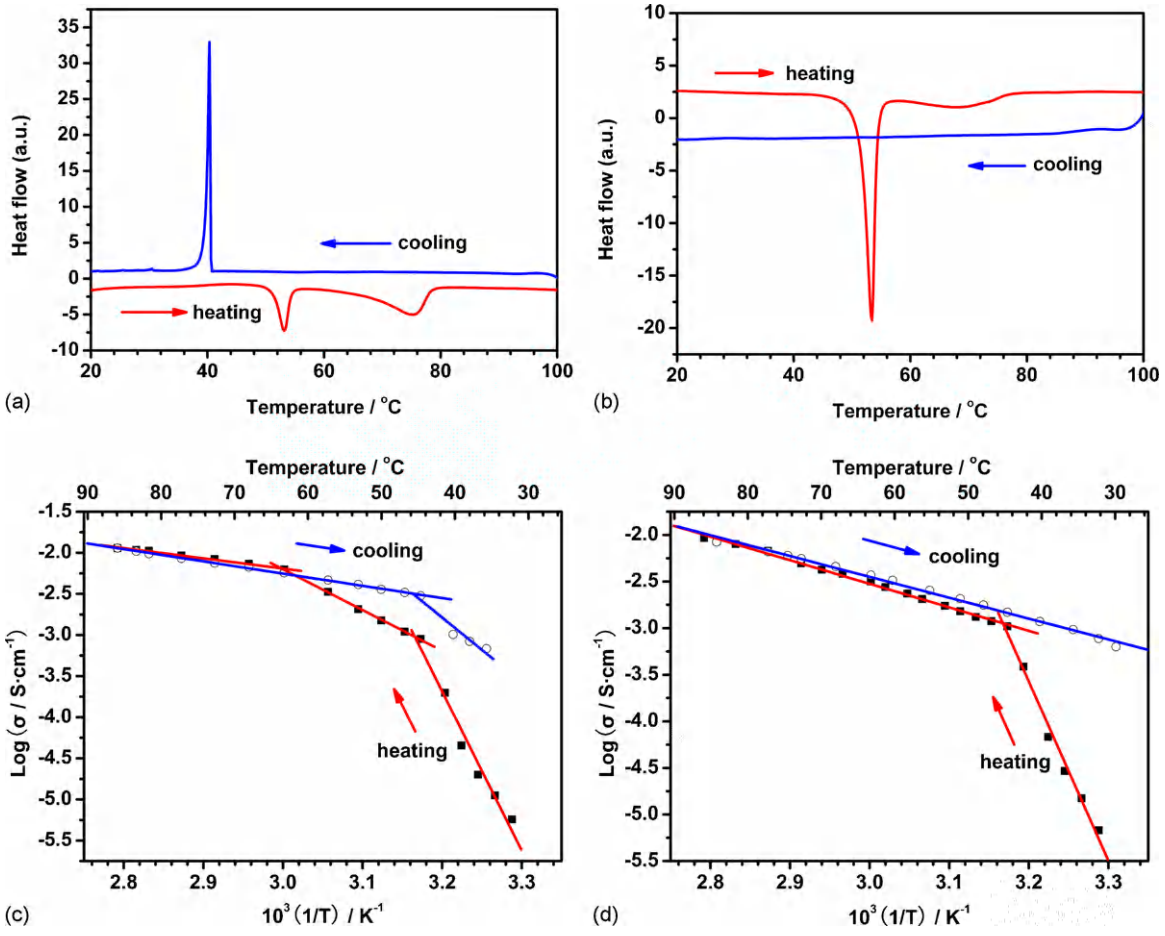

Fig. 5. (a) DSC curves of electrolyte A; (b) DSC curves of electrolyte D; (c) Arrhenius plots of electrolyte A; (d) Arrhenius plots of electrolyte D.

Table 2
Detailed parameters of the DSSC fabricated with the electrolyte A at different temperatures.

Temperature (°C)	J_{sc} (mA cm^{-2})	V_{oc} (mV)	*FF*	η (%)
30	0.267	501	0.364	0.049
35	0.347	508	0.395	0.070
40	0.613	535	0.375	0.123
45	0.773	530	0.378	0.155
50	1.27	553	0.447	0.313
55	1.79	556	0.472	0.468
60	2.29	548	0.494	0.622
65	2.97	541	0.506	0.813
70	3.45	523	0.561	1.014
75	4.91	508	0.586	1.461
80	5.40	474	0.592	1.515
85	5.24	438	0.600	1.377

J_{sc}: short circuit current density; V_{oc}: open circuit voltage; *FF*: fill factor; η: overall energy conversion efficiency.

of the redox potential (I_3^-/I^-) in the electrolyte [33]. The *FF* (fill factor) presents increasing trend almost in the whole temperature range. An efficiency of 1.52% at 80 °C was obtained.

The light to electricity conversion efficiency of our phase transition electrolyte DSSC is very low, especially at room temperature. This is not only related to sluggish diffusion kinetics of redox couples, but also related to poor contact between the TiO_2 anode and the electrolyte, which is the common disadvantage for solid-state electrolytes [34]. Owing to the rapid crystallization process, the electrolyte tends to form large crystals and it is difficult to fully penetrate into the pores of the TiO_2 film. As a result, some interface regions of the TiO_2 are naked without being wetted by the electrolyte. In the absence of the electrolyte, the injected conduction band electrons can be recaptured by the oxidized dye molecules before being extracted to the external circuit [35]. Consequently, the dark current increases and the V_{oc} is low. Therefore, good interfacial contact is crucial to reduce the above dark current. According to our previous researches, some ceramic oxides, such as SiO_2, TiO_2, and Al_2O_3, are very effective to suppress the crystallization

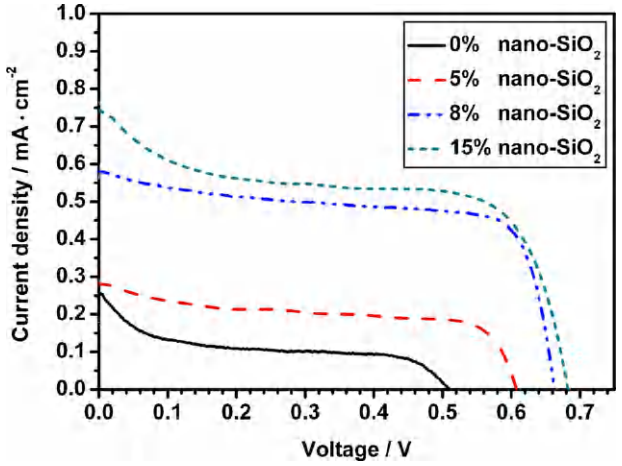

Fig. 6. *I–V* curves of the DSSCs fabricated with the electrolytes A (1:16) containing different amounts of nano-SiO_2 at 30 °C.

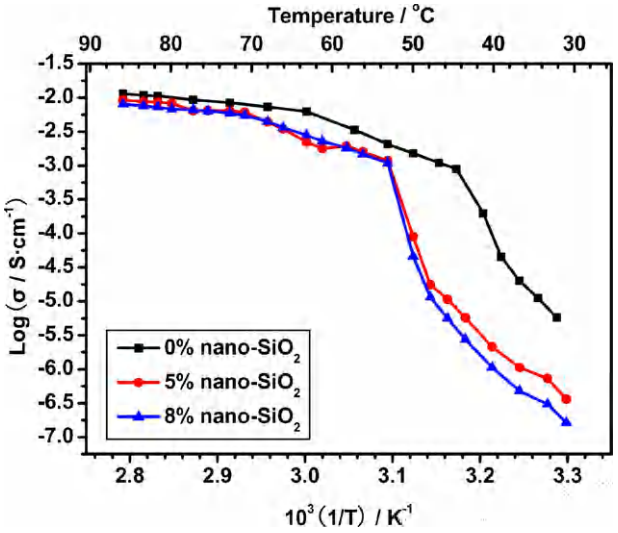

Fig. 8. Temperature-dependent conductivities of the electrolytes A with different amounts of nano-SiO_2.

of solid electrolyte or polymer electrolyte [19,36,37] and improve the interfacial contact. In this case, nano-SiO_2 particles (Degussa A150, 14 nm) is selected as the additive and the performances of the DSSCs with electrolytes A (1:16) containing different nano-SiO_2 contents are shown in Figs. 6 and 7.

It is clearly from Figs. 6 and 7 that the V_{oc} has been greatly improved with the addition of nano-SiO_2 into the electrolyte both at room temperature and 75 °C. This phenomenon agrees well with our previous work [19]. Here the highest efficiency of 4.2% at 75 °C was obtained for the DSSC containing 8 wt% nano-SiO_2 in the electrolyte. Although the electrolyte containing 15 wt% nano-SiO_2 performs a little better at room temperature, it tends to be peeled off. Therefore, 8 wt% silica content was selected in the following experiments.

Fig. 8 presents the Arrhenius plots of the electrolytes (LiI/acetamide = 1:16) with different silica contents. Each curve shows three slopes. The conductivities of electrolytes containing 5 and 8 wt% nano-SiO_2 are 3.6×10^{-7} and 1.6×10^{-7} S cm^{-1} at 30 °C, respectively, much lower than that of electrolyte without silica. The conductivities of the electrolytes with nano-SiO_2 also decrease in the liquid regime slightly. While in the high temperature region, especially over 70 °C, the conductivity differences among the three samples are not significant. This phenomenon is different with the LiI/HPN solid electrolyte system and the $LiClO_4$/EC-DMC system [38]. In those cases, the conductivity of the electrolyte has been increased by introducing a certain amount of nano-SiO_2. The conductivity mechanism after adding nano-SiO_2 needs further clarification.

According to the above results, there is no positive effect of nano-SiO_2 on the conductivity of the electrolyte. Therefore, the improvement of the interfacial contact is the key factor in our system. To scrutinize the properties of the TiO_2/electrolyte interface, the *I–V* characteristics in dark and the EIS (electrochemical impedance spectroscopy) experiments are carried out further.

In the dark under forward bias, electrons are injected into the TiO_2 anode and transported through the mesoscopic TiO_2 network. Meanwhile, I^- is oxidized to I_3^- at the counter electrode and the formed tri-iodide diffuses to the TiO_2 electrode to capture the electrons from the porous film at the titania/electrolyte interface [39]. The net current density in this circuit can be largely depended on the applied bias voltage, and is affected significantly by the diffusion rate of tri-iodide ions in the electrolyte as well as the charge transfer impedance at the interfaces in the cell (mainly TiO_2/electrolyte and electrolyte/Pt).

I–V curves (measured in dark under forward bias at 30 °C) of DSSCs with different amount of nano-SiO_2 in the electrolytes (1:16) are illustrated in Fig. 9. When the bias voltage is small, e.g. below

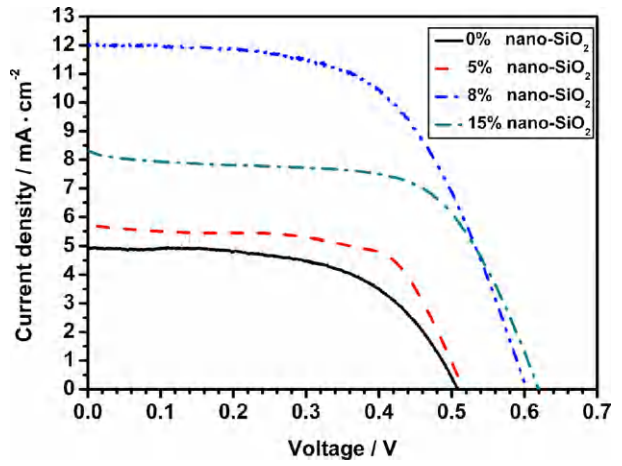

Fig. 7. *I–V* curves of the DSSCs fabricated with the electrolytes A (1:16) containing different amounts of nano-SiO_2 at 75 °C.

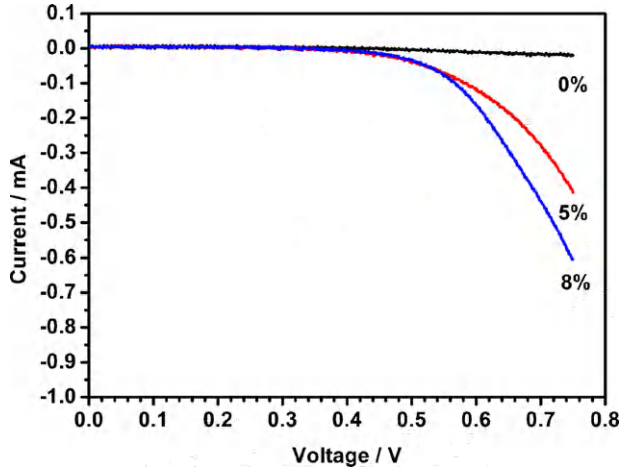

Fig. 9. *I–V* curves of DSSCs (in dark under forward bias at 30 °C) with different amount of nano-SiO_2 in the electrolyte.

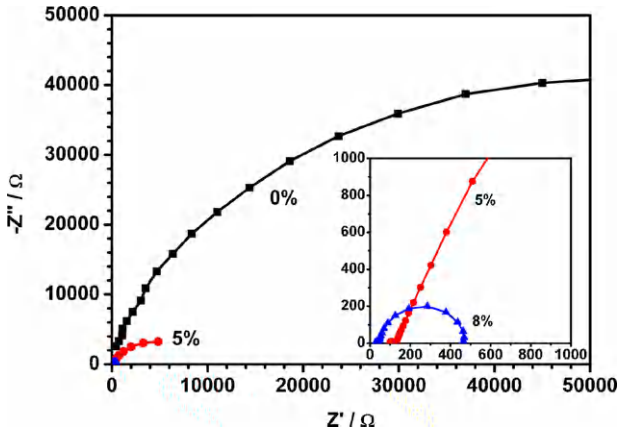

Fig. 10. Nyquist plots of the DSSCs fabricated with electrolytes A containing different amount of nano-SiO_2 in dark under −0.750 V. The inset shows the high frequency region of the spectra.

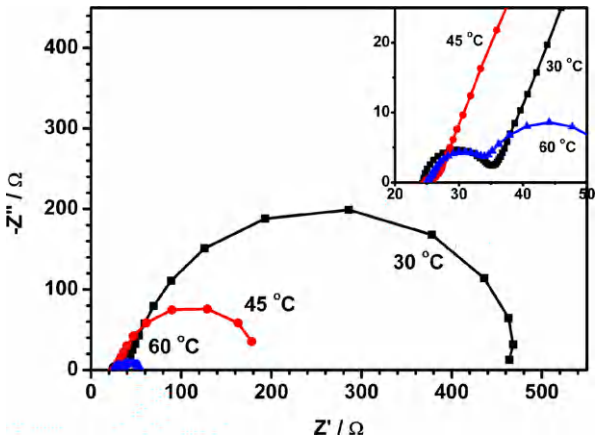

Fig. 12. Nyquist plots of the DSSC fabricated with electrolyte A containing 8 wt% nano-SiO_2 (in dark under −0.750 V) at different temperatures. The inset shows the high frequency region of the spectra.

0.4 V, the current seems to be zero and it increases remarkably (except for the sample without silica) when the forward bias is lager than 0.4 V, producing a response curve similar to a diode. This agrees with the work of Han et al. [40,41]. They described the TiO_2/electrolyte interface as a diode element in the DSSC by analyzing the equivalent circuit. Under the same bias voltage, as shown in Fig. 9, larger current has been obtained for the DSSC containing more silica in the electrolyte, suggesting the better interfacial contact and consequently the smaller charge transfer resistance (R_{ct}) at both the TiO_2/electrolyte and electrolyte/Pt interfaces. In the case of the DSSC without silica in the electrolyte, the current is negligible even at 0.75 V forward bias, which reveals large impedance at the interfaces mentioned above. The results are in agreement with the impedance spectra shown in Fig. 10. For the cell without nano-SiO_2 in the electrolyte, only one large arch is visible in the Nyquist diagram. When silica is added into the electrolyte, the diameter of the semicircle decreases significantly. This result indicates clearly that the electrode kinetics in this system is influenced strongly by the interfacial contact issue.

The influence of temperature on the dark current and impedance of the solar cell using 1:16 electrolyte containing 8 wt% nano-SiO_2 are also investigated and the results are shown in Figs. 11 and 12, respectively. When the temperature increases, the electrolyte melts and the interfacial contact is further improved. Meanwhile, the conductivity of the electrolyte is also increased by several orders of magnitude (see Fig. 8). As a result, the impedance at the solid/electrolyte interface and that in the electrolyte is reduced significantly (Fig. 12) and then the larger current has been obtained under the given voltage at the higher temperature, as shown in Fig. 11. When the temperature reaches 60 °C, the interfacial impedance decreases significantly that another small semicircle at high frequency can be seen clearly (see the inset of Fig. 12).

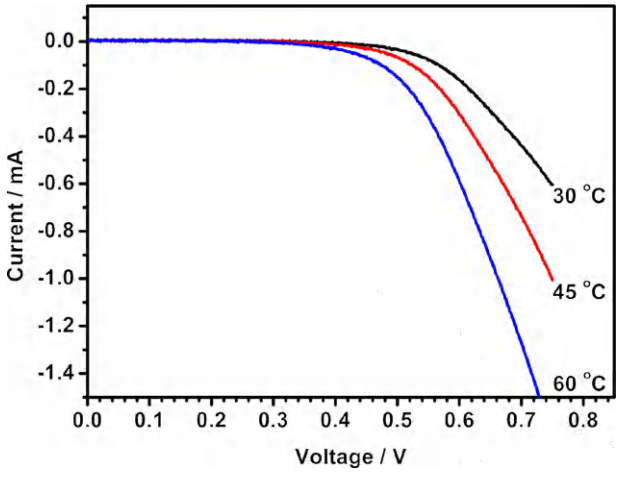

Fig. 11. *I–V* curves of DSSC (in dark under forward bias) with 8 wt% nano-SiO_2 in the electrolyte at different temperatures.

The morphologies of the electrolytes on the surface of TiO_2 film and the cross sectional SEM images are investigated. Fig. 13(a) shows the surface morphology of the TiO_2 film we used. The diameter of the P25 particle is around 21 nm and some large particles of about 150 nm were added to scatter the incident light. From Fig. 13(b), it can be seen clearly that most of the porous film surface was covered by the electrolyte and big crystals of several micrometers are formed. Fig. 13(c) shows the morphology of the electrolyte containing 8 wt% nano-SiO_2. Apparently, the addition of silica hinders the crystallization of LiI/acetamide electrolyte and no big crystals can be found in large scale. Uniform composite electrolyte with smaller particle size is formed. Fig. 13(e) illustrates the cross section view of the TiO_2 film with electrolyte A. It shows no prominent difference with the bare TiO_2 film displayed in Fig. 13(d). The nanoparticles and the pores are distinguishable. After introducing the silica, the permeation of the electrolyte into the pores of the film is much better due to the inhibition of the crystallization, as shown in Fig. 13(f). The penetration of the solid electrolyte and the nano-silica into the nanoporous P25 electrode has already been confirmed by the SEM/EDX experiment (not shown here). In Fig. 13(f), most of the TiO_2 particles are covered by the electrolyte. Therefore, the filling of solid electrolyte within the porous structure of the TiO_2 electrode and the electrode/electrolyte contact are greatly improved, as also evidenced by dark current and EIS experiment. Since the interfacial charge transfer is improved, consequently, the loss of injected electrons through recombination with the dye cations is effectively confined and the V_{oc} has been improved by continuous injection of electrons from the excited state of the dye to the conduction band of TiO_2.

3.5. Dependence of J_{sc} of DSSC fabricated with LiI/acetamide electrolyte (1:16) containing 8 wt% silica on incident power intensity

Fig. 14 shows the dependence of J_{sc} on the incident power intensity at 30 and 70 °C, respectively. When the temperature is low, the J_{sc} does not increase with the increasing radiation power linearly especially at higher light intensity. The photocurrent seems to be saturated when the radiation power is larger than 40 mW cm^{-2}. At

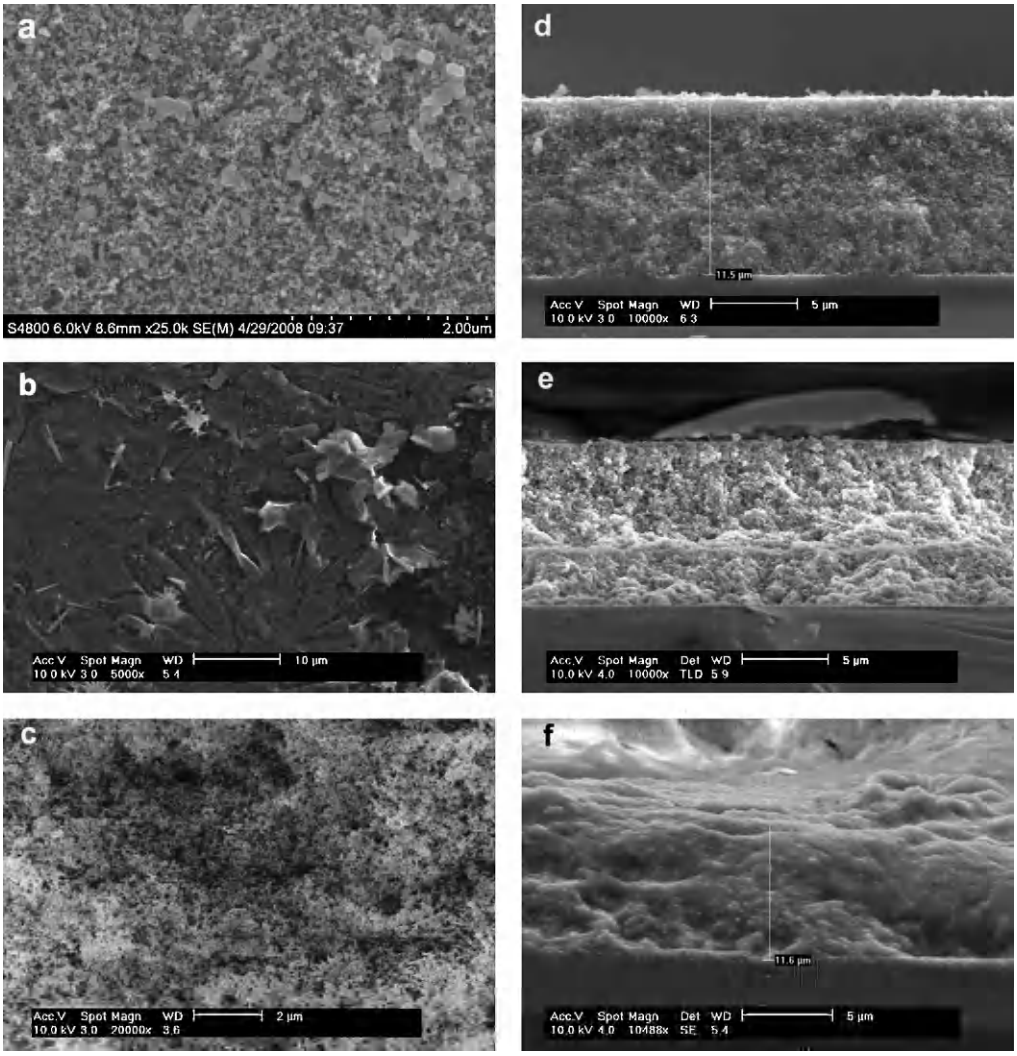

Fig. 13. Morphologies of (a) surface of bare TiO_2 film; (b) electrolyte A on the TiO_2 film; (c) electrolyte A with 8 wt% nano-SiO_2 on the TiO_2 film; (d) cross section of bare TiO_2 film; (e) cross section of TiO_2 film with electrolyte A; and (f) cross section of TiO_2 film with electrolyte A containing 8 wt% nano-SiO_2.

this temperature (lower than the melting point), the electrolyte is in a solid form and the mass transport is rather slow. Therefore, the J_{sc} is limited by the diffusion of I_3^- and a nonlinear response is observed [42]. On the other hand, when the electrolyte is heated to 70 °C (higher than the melting point), it turns into liquid. As a result, the conductivity increases greatly as mentioned above and the diffusion of I_3^- becomes much easier. The photocurrent is only limited by the incident power intensity rather than the ionic mobility and then a nearly linear response of J_{sc} versus radiant power is observed.

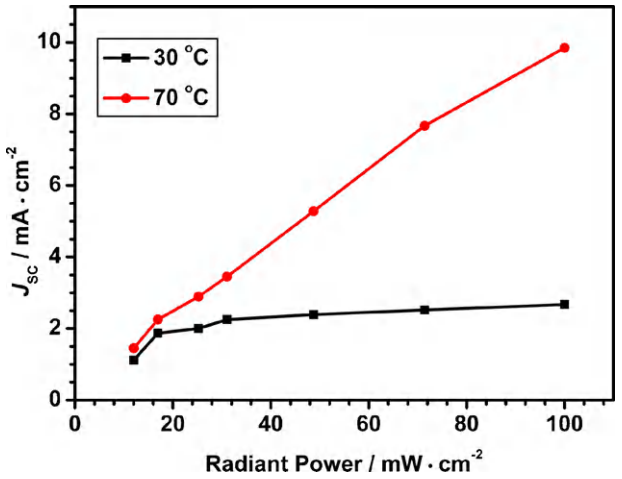

Fig. 14. J_{sc} versus radiation power for DSSC with LiI/acetamide electrolyte (1:16) containing 8 wt% silica at different temperatures.

3.6. The performance of the DSSC using this phase transition electrolyte at different temperatures

The *I–V* curves of DSSC based on the electrolyte A containing 8 wt% nano-SiO_2 are illustrated in Fig. 15. The performances at 35 and 75 °C are J_{sc} = 0.667 mA cm^{-2}, V_{oc} = 656 mV, FF = 0.711 and J_{sc} = 12.0 mA cm^{-2}, V_{oc} = 602 mV, FF = 0.581, respectively. The total efficiency is increased from 0.3 to 4.2%. With the further increasing temperature, nevertheless, the η decreases due to the significant drop of both the photocurrent and voltage.

For DSSCs with common liquid electrolyte, they perform best at ambient conditions and the J_{sc} as well as the efficiency will decline at high temperature mainly due to the recombination and the voltage drop [33]. In our system, the high temperature gives rise to an increase of the ionic conductivity of the electrolyte and improves the electrode/electrolyte contact. Thus the J_{sc} and overall conversion efficiency are enhanced. The peak value of the J_{sc} and the

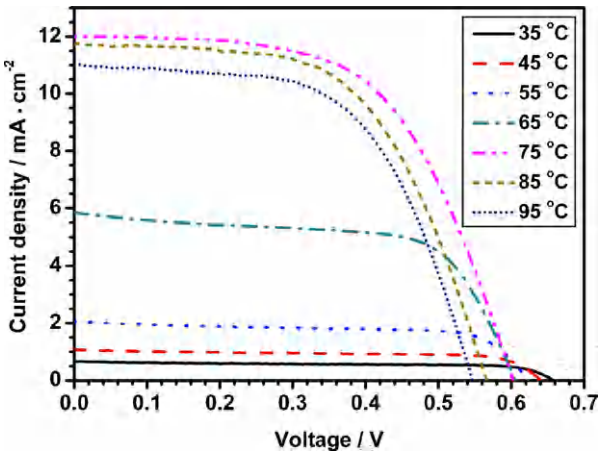

Fig. 15. Photocurrent–voltage characteristics of DSSC fabricated with optimized electrolyte (1:16, 8 wt% nano-SiO_2) under AM 1.5 illumination (100 mW cm^{-2}) at different temperatures.

highest efficiency appear at about 75 °C, which is more suitable for DSSCs in view of outdoor practical application under hot weather.

We note that the V_{oc} decreases monotonously with the increasing temperature. This is different from the case of electrolyte without silica. In the latter case, the V_{oc} rose initially since the improvement of the interfacial contact after heating (Table 2). Then electron loss is increased at higher temperature and the V_{oc} declines. They are two competitive processes and a peak value appears. While for the DSSC with 8 wt% silica in the electrolyte, the contact between TiO_2 and electrolyte is good even at room temperature and the back reaction becomes the dominant factor. Finally, the V_{oc} decreases monotonously.

Although the achieved efficiency is not competitive to current state-of-the-art DSSC and need further optimization, current preliminary results show interesting features of the DSSC using phase transition electrolyte. It could show high stability during long term storage at cool night and high operation efficiency at hot daytime.

4. Conclusions

A new series of solid electrolytes composed of LiI and acetamide are synthesized. The melting points are around 50 °C so that these electrolytes act as phase transition electrolytes. The performances of the DSSCs assembled with these electrolytes are not satisfactory mainly due to poor contact of the electrolyte with the porous TiO_2 electrode especially at room temperature. Addition of nanosized SiO_2 particles into the electrolyte improves the interfacial contact significantly. Consequently, using an optimized composite electrolyte to fabricate DSSC, efficiency of 0.3 and 4.2% were achieved under 1 sun illumination at 35 and 75 °C, respectively. Although the efficiency is not high enough, the feasibility of DSSC using the phase transition electrolyte is shown for the first time and it may be suitable for outdoor practical applications under environment with large temperature difference during daytime and night and should be more stable during storage under dark and cool environment, needing further investigation. It is plausible that the melting point of the electrolytes could be tuned by changing the components of the electrolyte as well as the molar ratio to match the requirements. Electrolytes with higher conductivity and better performance are further pursued.

Acknowledgments

This work was supported by the National Natural Science Foundation of China (Grants 20725311, 20673141, 20703063, and 20721140647), the Ministry of Science and Technology of China (973 Project, 2006CB202606, 2007CB936501) and (863 Project, Grant 2006AA03Z341), the Strategic China-Japan (NSFC-JST) Joint Research Program, and the 100 Talent Project of the Chinese Academy of Sciences.

References

[1] B. O'Regan, M. Grätzel, Nature 353 (1991) 737.
[2] M. Grätzel, J. Photochem. Photobiol. A 164 (2004) 3.
[3] J.M. Kroon, N.J. Bakker, H.J.P. Smit, P. Liska, K.R. Thampi, P. Wang, S.M. Zakeeruddin, M. Grätzel, A. Hinsch, S. Hore, U. Würfel, R. Sastrawan, J.R. Durrant, E. Palomares, H. Pettersson, T. Gruszecki, J. Walter, K. Skupien, G.E. Tulloch, Prog. Photovolt. Res. Appl. 15 (2007) 1.
[4] K. Tennakone, G.R.R.A. Kumara, A.R. Kumarasinghe, K.G.U. Wijayantha, P.M. Sirimanne, Semicond. Sci. Technol. 10 (1995) 1689.
[5] K. Tennakone, V.P.S. Perera, I.R.M. Kottegoda, G.R.R.A. Kumara, J. Phys. D-Appl. Phys. 32 (1999) 374.
[6] Q.-B. Meng, K. Takahashi, X.-T. Zhang, I. Sutanto, T.N. Rao, O. Sato, A. Fujishima, Langmuir 19 (2003) 3572.
[7] U. Bach, D. Lupo, P. Comte, J.-E. Moser, F. Weissorter, J. Salbeck, H. Spreitzer, M. Grätzel, Nature 395 (1998) 583.
[8] H.J. Snaith, A.J. Moule, C. Klein, K. Meerholz, R.H. Friend, M. Grätzel, Nano Lett. 7 (2007) 3372.
[9] W. Kubo, K. Murakoshi, T. Kitamura, Y. Wada, K. Hanabusa, H. Shirai, S. Yanagida, Chem. Lett. 27 (1998) 1241.
[10] W. Kubo, K. Murakoshi, T. Kitamura, S. Yoshida, M. Haruki, K. Hanabusa, H. Shirai, Y. Wada, S. Yanagida, J. Phys. Chem. B 105 (2001) 12809.
[11] O.A. Ileperuma, M.A.K.L. Dissanayake, S. Somasundaram, Electrochim. Acta 47 (2002) 2801.
[12] R. Komiya, L. Han, R. Yamanaka, A. Islam, T. Mitate, J. Photochem. Photobiol. A-Chem. 164 (2004) 123.
[13] L. Wang, S.B. Fang, Y. Lin, X.W. Zhou, M.Y. Li, Chem. Commun. (2005) 5687.
[14] P.J. Li, J.H. Wu, M.L. Huang, S.C. Hao, Z. Lan, Q.H. Li, S.J. Kang, Electrochim. Acta 53 (2007) 903.
[15] W.C. Xiang, Y.F. Zhou, X. Yin, X.W. Zhou, S.B. Fang, Y. Lin, Electrochim. Acta 54 (2009) 4186.
[16] B.F. Xue, H.X. Wang, Y.S. Hu, H. Li, Z.X. Wang, Q.B. Meng, X.J. Huang, L.Q. Chen, O. Sato, A. Fujishima, Chin. Phys. Lett. 21 (2004) 1828.
[17] B.F. Xue, H.X. Wang, Y.S. Hu, H. Li, Z.X. Wang, Q.B. Meng, X.J. Huang, O. Sato, L.Q. Chen, A. Fujishima, Photochem. Photobiol. Sci. 3 (2004) 918.
[18] H.X. Wang, B.F. Xue, Y.S. Hu, Z.X. Wang, Q.B. Meng, X.J. Huang, L.Q. Chen, Electrochem. Solid-State Lett. 7 (2004) A302.
[19] H.X. Wang, H. Li, B.F. Xue, Z.X. Wang, Q.B. Meng, L.Q. Chen, J. Am. Chem. Soc. 127 (2005) 6394.
[20] H.X. Wang, Z.X. Wang, H. Li, Q.B. Meng, L.Q. Chen, Electrochim. Acta 52 (2007) 2039.
[21] N. Papageorgiou, Y. Athanassov, M. Armand, P. Bonhote, H. Pettersson, A. Azam, M. Grätzel, J. Electrochem. Soc. 143 (1996) 3099.
[22] P. Wang, S.M. Zakeeruddin, J.-E. Moser, M. Grätzel, J. Phys. Chem. B 107 (2003) 13280.
[23] Y. Bai, Y.M. Cao, J. Zhang, M.K. Wang, R.Z. Li, P. Wang, S.M. Zakeeruddin, M. Grätzel, Nat. Mater. 7 (2008) 626.
[24] Y.S. Hu, H. Li, X.J. Huang, L.Q. Chen, Electrochem. Commun. 6 (2004) 28.
[25] Y.S. Hu, Z.X. Wang, H. Li, X.J. Huang, L.Q. Chen, Spectrochim. Acta Part A 61 (2005) 2009.
[26] Y.S. Hu, Z.X. Wang, X.J. Huang, L.Q. Chen, Solid State Ionics 175 (2004) 277.
[27] B. Xie, L.F. Li, H. Li, L.Q. Chen, Solid State Ionics 180 (2009) 688.
[28] M.K. Nazeerudin, A. Kay, I. Rodicioet, R. Humpbry-Baker, E. Miiller, P. Liska, N. Vlachopoulos, M. Grätzel, J. Am. Chem. Soc. 115 (1993) 6382.
[29] R.J. Chen, F. Wu, Acta Phys.-Chim. Sin. 21 (2005) 177.
[30] Y.S. Hu, Z.X. Wang, H. Li, X.J. Huang, L.Q. Chen, Spectrochim. Acta Part A 61 (2005) 403.
[31] M. Dürr, G. Kron, U. Rau, J.H. Werner, A. Yasuda, G. Nelles, J. Chem. Phys. 121 (2004) 11374.
[32] G. Berchiesi, J. Mol. Liq. 83 (1999) 271.
[33] S.H. Chen, J. Weng, S.Y. Dai, Y.F. He, K.J. Wang, Acta Energiae Solaris Sinica 27 (2006) 900.
[34] B. Li, L.D. Wang, B.N. Kang, P. Wang, Y. Qiu, Sol. Energy Mater. Sol. Cells 90 (2006) 549.
[35] S. Pelet, J.-E. Moser, M. Grätzel, J. Phys. Chem. B 104 (2000) 1791.
[36] K.-S. Ji, H.-S. Moon, J.-W. Kim, J.-W. Park, J. Power Sources 117 (2003) 124.
[37] F. Croce, G.B. Appetecchi, L. Persi, B. Scrosati, Nature 394 (1998) 456.
[38] A.J. Bhattacharyya, J. Maier, Adv. Mater. 16 (2004) 811.
[39] Q. Wang, J.-E. Moser, M. Grätzel, J. Phys. Chem. B 109 (2005) 14945.
[40] L.Y. Han, N. Koide, Y. Chiba, T. Mitate, Appl. Phys. Lett. 84 (2004) 2433.
[41] N. Koide, A. Islam, Y. Chiba, L.Y. Han, J. Photochem. Photobiol. A-Chem. 182 (2006) 296.
[42] S.Y. Huang, G. Schlichthörl, A.J. Nozik, M. Grätzel, A.J. Frank, J. Phys. Chem. B 101 (1997) 2576.